

Low-momentum K^+d scattering*

R. G. Glasser, G. A. Snow, and D. Trevett†
 University of Maryland, College Park, Maryland 20742

R. A. Burnstein, C. Fu, , R. Petri, G. Rosenblatt,† and H. A. Rubin
 Illinois Institute of Technology, Chicago, Illinois 60616
 (Received 13 September 1976)

The differential cross sections for K^+d coherent, breakup, and charge-exchange scattering have been measured at several momenta in the interval 250–600 MeV/c. The data have been fitted using a partial-wave analysis. Assuming an s -wave description of $I = 1$ scattering and using data from the coherent and charge-exchange channels, a description of $I = 0$ K^+N scattering by a combination of s and p waves in a simple single-scattering impulse model has been attempted. The phase shifts obtained are unique up to the Fermi-Yang ambiguity, which can be removed by using existing polarization results at 600 MeV/c.

I. INTRODUCTION

In recent years total and partial cross-section measurements on the K^+ -nucleon system have shown structure in both the isospin $I=0$ and $I=1$ channels.¹⁻⁶ Considerable interest has been focused on the question of whether this structure is evidence of the existence of strangeness +1 resonances. Such resonances would be exotic since they cannot be represented by a simple three-quark wave function.⁷

Both energy-dependent and energy-independent phase-shift analyses have been performed by numerous groups on the existing differential-cross-section distributions.⁸⁻¹² These analyses can be greatly aided by accurate low-energy scattering data, which provide anchor points for the low-angular-momentum partial waves. To improve knowledge of the K^+ -nucleon system in this low-energy region, measurements of K^+p and K^+d scattering were made at four momenta below 600 MeV/c. The results of the K^+p analysis have previously been published.¹³

In the low-energy region pion production is negligible, and only the following three K^+d reactions need to be considered:

$$K^+ + d \rightarrow K^+ + d \quad (\text{coherent}) \quad (1.1)$$

$$K^+ + d \rightarrow K^+ + p + n$$

(breakup without charge exchange) (1.2)

$$K^+ + d \rightarrow K^0 + p + p$$

(breakup with charge exchange). (1.3)

The last two will be referred to simply as breakup and charge exchange, respectively.

II. EXPERIMENTAL METHOD

The experiment was performed at the Brookhaven National Laboratory alternating gradient

synchrotron (AGS) using the low-energy separated K beam¹⁴ at a transport momentum of 614 MeV/c. Data was taken in the BNL-Columbia 30-in. bubble chamber filled with deuterium, at four incident momenta produced by placing varying lengths of copper degrader just in front of the bubble chamber. Sample distributions of beam momenta at interaction vertices are shown in Fig. 1. The ex-

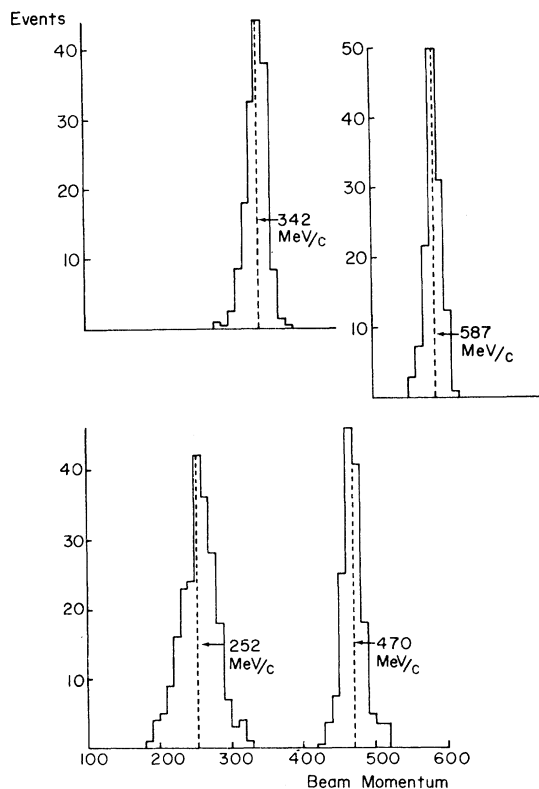


FIG. 1. The distribution of beam momenta at the charge-exchange interaction vertex. The mean momentum is indicated for each data set.

TABLE I. Summary of K^+d exposure.

Beam momentum ^a (MeV/c)	Path length ^e	Events/mb	Beam acceptance criteria ^f						τ count
			Momentum (MeV/c)		Beam dip (deg)		Azimuth (deg) ^g		
			Min	Max	Min	Max	Min	Max	
587 ± 12 ^b	4.38 ± 0.30 × 10 ⁶	58.6	550	628	-4.5	3.1	101.6	115.3	555 ± 38
587 ± 12 ^c	2.05 ± 0.27 × 10 ⁶	84.8	550	628	-4.5	3.1	101.6	115.3	260 ± 30
470 ± 12 ^b	5.02 ± 0.28 × 10 ⁶	68.0	424	514	-6.8	5.8	100.8	127.2	797 ± 45
470 ± 12 ^d	2.93 ± 0.15 × 10 ⁶	130.3	440	570	-11	11	81	115	463 ± 23
342 ± 15 ^b	8.13 ± 0.44 × 10 ⁶	106.1	286	386	-7.9	5.7	104.0	36.1	1769 ± 95
342 ± 15 ^d	2.64 ± 0.12 × 10 ⁶	109.2	340	445	-11	11	80	117	577 ± 25
252 ± 25 ^b	8.19 ± 0.45 × 10 ⁶	116.7	184	328	-9.4	7.6	109.7	141.8	2420 ± 125

^aAt central plane of bubble chamber.

^bAnalyzed at IIT for charge-exchange scatters.

^cAnalyzed at IIT for coherent and breakup scatters.

^dAnalyzed at Maryland for coherent and breakup scatters (all τ 's measured for these samples).

^eSee text, Sec. II C.

^fThese cuts made on results of geometric reconstruction, not on kinematically fitted results. IIT cuts made at the central plane. Maryland cuts made at the entrance plane.

^gProjected beam angle.

posure totaled about 214 000 pictures distributed over the four momenta 587, 470, 342, and 252 MeV/c.

There were approximately eleven beam tracks per frame. A typical beam-kaon track (at 470 MeV/c) had a bubble density of about 10 bubbles per cm. This choice of bubble density allowed good visual ionization discrimination between K^+ and π^+ for all but the highest momentum covered by the experiment. In that case, the beam pions, which constitute about a 2.5% contaminant, were eliminated to the level of $\leq 1\%$ by the application of the beam acceptance criteria summarized in Table I. These criteria were applied at all momenta, with the result that the purity of the beam was independent of the scanning criteria.

A. Scan and measurement

Independent sets of scans were performed for the different topologies: one set picked up charge-exchange events [reaction (1.3)] and 3-prong K decays (the latter used for normalization), while the other was devoted to 2-prong K scatters [reactions (1.1) and (1.2)]. Each set consisted of at least two scans, with a portion of the film used for charge exchange and normalization receiving a third scan. The scanning efficiencies as determined by comparing multiple scans for the various topologies are all >99%; systematic losses are discussed in Sec. II D.

Measurements and remeasurements were performed on standard film-plane and image-plane

machines. All data analysis was performed with a standard chain^{15,16} of bubble-chamber-analysis programs, TVGP, SQUAW, and ARROW, on Univac 1108 computers at Maryland and IIT using essentially identical programs.

B. Parameters of the experiment

The liquid-deuterium density was determined by measuring the range of μ^+ produced by stopping π^+ via the decay $\pi^+ \rightarrow \mu^+ + \nu$. The π^+ decays were obtained from a sample of τ decays ($K^+ \rightarrow \pi^+ + \pi^+ + \pi^-$) at all momenta. The mean μ^+ range was found to be 0.934 ± 0.005 cm, which implied a deuterium density $\rho_D = 0.139 \pm 0.001$ g/cm³. The central magnetic field was 12.75 ± 0.13 kG, based on magnet-current readings during the run. This is in reasonable agreement with an independent determination of the magnetic field based on kinematic fitting.^{17,18}

C. Path length

The K^+ path length was determined for each of the different momentum intervals from the number of observed τ decays at that momentum. The path length in centimeters is given by

$$L = (p/M) \times ct \times N_\tau / B,$$

where p and M are the momentum and the mass of the decaying K^+ expressed in MeV/c and MeV/c², respectively, $ct = 370.8 \pm 0.8$ cm is the K^+ lifetime,¹⁹ N_τ is the number of τ decays, and $B = 0.0559 \pm 0.0003$ is the τ -decay branching ratio.¹⁹

The K^+ path length and the total number of τ decays for each momentum interval and topology are listed in Table I.

D. Data-sample selection criteria and corrections

1. Charge-exchange sample

The charge-exchange data sample was obtained from events fitting reaction (1.3). The scanning criteria required the identification of an incoming K^+ , one or two outgoing (proton) tracks from the primary vertex, and a "V" within about 30 cm of this vertex. Only those charge-exchange events in which a K^0_{short} decayed into a charged-pion pair were recorded in this category. The known branching ratio for this K^0 decay mode (0.3439 ± 0.0026)¹⁹ was then used to determine the total number of K^0 produced in each angular region. Only those events with K^0 length less than 20.00 cm and projected K^0 length greater than 0.25 cm were included in the final charge-exchange sample. Events fulfilling these criteria were, in general, well constrained. Each event was weighted by the inverse of the probability that a K^0 with the momentum observed would have decayed within the length interval given above, to correct for events excluded by the cuts.

Overall corrections were also made for scanning losses (<1% at all momenta) and for the loss of events which, although passing geometric cuts and positively identified as charge-exchange scatters, failed to produce good kinematic fits to this hypothesis (about 7% of the events). The correction factor for these lost events was obtained by calculating the ratio of the total number of events to the total number of well-fitted events (~1.07). A test of azimuthal symmetry in all relevant distributions failed to reveal any statistically significant deviations from isotropy. Therefore, no additional geometric weights have been applied to the charge-exchange sample.

Our measured K^0 lifetime is $(0.90 \pm 0.03) \times 10^{-10}$ sec, which agrees with the accepted value of $(0.882 \pm 0.008) \times 10^{-10}$ sec.¹⁹

2. Coherent and breakup sample

The coherent and breakup sample was obtained from events fitting either reaction (1.1) or reaction (1.2), or both. The scanning criteria for these events required the identification of all 2-prong events with no associated "V"; there were no minimum or maximum length restrictions on any of the tracks, nor was the outgoing proton (deuteron) required to stop in the chamber. Measurements were made of all events which could have been consistent with coherent or breakup

scattering. Most kinematic ambiguities in these events could be resolved by a visual check of the relative ionizations of the tracks; the major exceptions were events with good fits to both coherent and breakup scattering.

There are several sources of difficulty in separating coherent and breakup scattering events. First, with the exception of high-momentum-transfer events in which the recoil length exceeds 25 cm, both proton and deuteron tracks are saturated and cannot be distinguished by ionization. In addition, most events which have kinematic fits to the coherent hypothesis also have fits to the breakup reaction. In the case of such ambiguous fits, one generally favors the coherent fits because they are far better constrained: 4 (or 3) constraints compared to 1 (or 0), where the numbers in parentheses apply if one of the measurable quantities of the event is undetermined (e.g., the momentum of one outgoing track, as with a secondary scatter close to the primary vertex). A study of the confidence-level distributions for coherent, breakup, and τ -decay fits at 342 and 470 MeV/c showed a large excess of low-confidence-level events only in the coherent sample, indicating a possible contamination in this sample owing to the presence of misidentified breakup scatters. An examination of coherent and breakup fits to large-momentum transfer events at 470 MeV/c, where protons and deuterons could be distinguished, supported the interpretation that the low-confidence-level fits in the coherent sample were indeed due to a contamination of breakup events. Therefore, a $\geq 2\%$ confidence-level fit for the coherent-scatter sample was required at 342 and 470 MeV/c. The events which were eliminated (8% of the coherent events at 342 MeV/c and 6% at 470 MeV/c) were transferred to the breakup-scatter sample. At 587 MeV/c no such effect was noted.

We have made further tests to determine whether the coherent-scatter sample contains any additional contamination due to breakup scatters. Any breakup events which are contaminants to the coherent sample fall in a restricted region of the total phase space available to the breakup events. In particular, since one expects true coherent scatters to have breakup fits with final-state nucleons that are approximately collinear and have low relative momentum, one also expects that false coherent events (from the breakup sample) will have these same properties. With this feature expected, we studied the distribution of the invariant mass of the p - n system, the collinearity of the final-state nucleons, the relative p - n momentum, and the transverse-momentum imbalance. We found¹⁸ that the best measure of the contamination

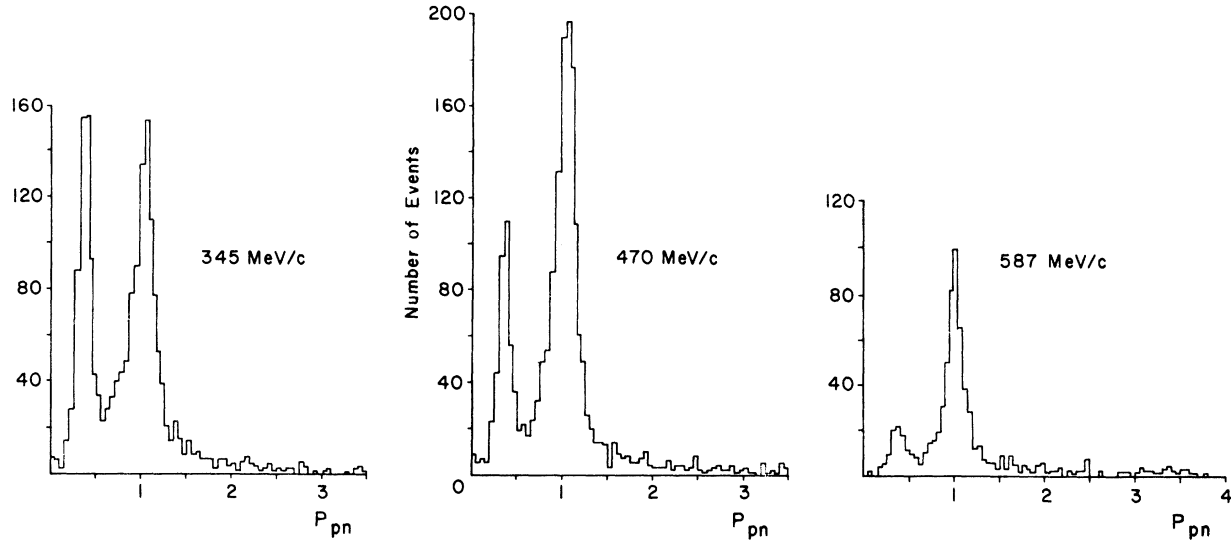


FIG. 2. Distribution of the normalized relative proton-neutron momentum ($P_{pn} = |\vec{p} - \vec{n}|/|\vec{p}|$) for all events with fits to the breakup hypothesis.

could be obtained by using the normalized p - n relative momentum, defined by $P_{pn} = |\vec{p} - \vec{n}|/|\vec{p}|$. If a stopping deuteron is misinterpreted as a proton, it is assigned a momentum equal to 0.6 times the deuteron value. The (collinear) neutron must have the rest of the deuteron moment, $0.4 \vec{d}$, leading to a prediction of $P_{pn} = \frac{1}{3}$ for true elastic events (or slightly larger if the proton and neutron are not exactly collinear). For nonstopping tracks, of course, the proton will be assigned a value of momentum closer to that of the deuteron, with the neutron having correspondingly less momentum; for these events P_{pn} will be closer to unity.

The P_{pn} distributions are shown in Fig. 2; the elastic peak occurs at $P_{pn} = 0.36$. The small cluster of events at zero primarily corresponds to events in which the deuteron momentum had been lost; if the K^+ was well measured in such cases, the breakup solution often shared the deuteron momentum equally between the two nucleons. As noted above the prediction of $P_{pn} \approx \frac{1}{3}$ for true elastics requires well-measured tracks, which implies that the deuteron momentum must have been determined from a range measurement; for other events, the value of P_{pn} is less well determined. This accounts for most of the elastics with $P_{pn} > 0.7$.

By making extrapolations from the breakup distribution into the coherent peak one can obtain estimates of the breakup contamination in the coherent sample. The elastic sample has on the average no contamination but has an error of 5% at 342 MeV/c, 7% at 470 MeV/c, and 9% at 587 MeV/c.

TABLE II. Laboratory coherent differential-cross-section data. These differential cross sections do not include the overall normalization error, which is $\pm 5\%$ at 342 and 470 MeV/c, and $\pm 10\%$ at 587 MeV/c.

$\cos\theta$ interval	No. of events	Correction factor	$d\sigma/d\Omega$ (mb/srad)
587 MeV/c			
(-1.0, -0.4)	9	1.0	0.028 ± 0.003
(-0.4, +0.25)	6	1.0	0.018 ± 0.006
(0.25, 0.5)	7	1.0	0.054 ± 0.017
(0.5, 0.75)	17	1.0	0.13 ± 0.03
(0.75, 0.85)	18	1.0	0.36 ± 0.09
(0.85, 0.90)	18	1.0	0.69 ± 0.18
(0.9, 0.95)	28	1.43 ± 0.08	1.54 ± 0.30
470 MeV/c			
(-1.0, -0.7)	7	1.0	0.031 ± 0.012
(-0.7, -0.4)	19	1.0	0.083 ± 0.019
(-0.4, -0.2)	10	1.0	0.066 ± 0.021
(-0.2, 0.0)	10	1.0	0.066 ± 0.021
(0.0, 0.2)	14	1.0	0.092 ± 0.024
(0.2, 0.4)	25	1.0	0.16 ± 0.03
(0.4, 0.6)	38	1.0	0.25 ± 0.04
(0.6, 0.8)	93	1.16 ± 0.04	0.71 ± 0.08
(0.8, 0.9)	114	1.24 ± 0.06	1.86 ± 0.20
(0.9, 0.95)	71	1.50 ± 0.12	2.80 ± 0.40
342 MeV/c			
(-1.0, -0.7)	22	1.0	0.11 ± 0.02
(-0.7, -0.4)	29	1.0	0.14 ± 0.03
(-0.4, -0.2)	22	1.0	0.16 ± 0.03
(-0.2, 0.0)	29	1.0	0.21 ± 0.04
(0.0, 0.2)	32	1.0	0.23 ± 0.04
(0.2, 0.4)	58	1.0	0.42 ± 0.06
(0.4, 0.6)	93	1.0	0.68 ± 0.07
(0.6, 0.8)	159	1.0	1.16 ± 0.09
(0.8, 0.9)	113	1.24 ± 0.06	2.05 ± 0.22

Of those events eventually identified as breakup scatters, about 7.5% (at each momentum) produced good charge-exchange fits which could not be excluded even by ionization checks. However, most of these involved steep outgoing tracks, so that a K^+ track would appear as saturated as a proton track. By using the azimuthal symmetry of both breakup and charge-exchange scattering about the beam direction, one can study the events with less steep scattering planes to determine the probability that an event with the observed scattering angle would be a charge-exchange scatter. From this we estimate an upper limit on the charge-exchange contamination in any portion of the breakup angular distribution to be $\sim 2\%$.

However, since 1-prong coherent and breakup scatters were not identified in our scans, the small-angle-scatter regions of these latter distributions were excluded from the analysis. In contrast, the final sample of charge-exchange events includes the entire range of scattering angles. Cuts were made at K^+ scattering-angle cosines in the laboratory system of 0.90 for the 342-MeV/c sample and 0.95 for the other two momenta. A one-parameter model, based on the assumption that scanning losses were due primarily to small projected scattering angles, was then used to correct the remaining distributions for such losses. These corrections were important only for the coherent sample in restricted regions of the laboratory scattering angle: $\cos\theta > 0.8$ at 342 MeV/c (19%), $\cos\theta > 0.6$ at 470 MeV/c (18%), and $\cos\theta > 0.9$ at 597 MeV/c (10%), where the figures in

parentheses are the overall percentage corrections.

III. RESULTS AND ANALYSIS OF DATA

A. Differential cross sections

Calculations of the differential cross sections for reactions (1.1), (1.2), and (1.3) are summarized in Tables II–IV and plotted in Figs. 3–5. Note that the coherent and breakup data are presented in the laboratory frame and that the charge-exchange data are given in the K^+ -nucleon c.m. (center-of-mass system, where the nucleon is treated as being initially at rest in the lab). Figure 6 presents the coherent differential cross sections as a function of the square of the four-momentum transfer t ; for comparison, data from other experiments at nearby energies have also been included.^{20–22}

B. Impulse-approximation model

The theoretical treatment used to analyze the K^+ - d reactions in terms of K -nucleon phase shifts is essentially that of Stenger,¹⁰ except that in analyzing the coherent scattering, where the form of the deuteron wave function is particularly important, we have computed the deuteron form factor from the Reid hard-core wave function, including the d wave.²³ The single-scattering impulse-approximation (SSLA) expressions for the various differential cross sections are as follows, in the reference frames indicated:

$$\left. \frac{d\sigma^c}{d\Omega} \right|_{\text{lab}} = K \left\{ \left[S_s^2 \left(\frac{q}{2} \right) + S_Q^2 \left(\frac{q}{2} \right) \left| a_1 + a_c + \frac{a_1 + a_0}{2} \right|^2 + \frac{2}{3} S_M^2 \left(\frac{q}{2} \right) \left| b_1 + \frac{b_1 + b_0}{2} \right|^2 \right] \right\}, \quad (3.1)$$

$$\left. \frac{d\sigma^b}{d\Omega} \right|_{K^+N \text{ c.m.}} = \left[|a_1 + a_c|^2 + \left| \frac{a_1 + a_0}{2} \right|^2 + |b_1|^2 + \left| \frac{b_1 + b_0}{2} \right|^2 \right] I_0(\theta^*) + 2 \operatorname{Re} \left[\left(\frac{a_1^* + a_0^*}{2} \right) (a_1 + a_c) + \frac{1}{3} b_1 \left(\frac{b_1^* + b_0^*}{2} \right) \right] J_0(\theta^*), \quad (3.2)$$

$$\left. \frac{d\sigma^x}{d\Omega} \right|_{K^+N \text{ c.m.}} = \left[\left| \frac{a_1 - a_0}{2} \right|^2 + \frac{2}{3} \left| \frac{b_1 - b_0}{2} \right|^2 \right] [I_0(\theta^*) - J_0(\theta^*)] + \frac{1}{3} \left| \frac{b_1 - b_0}{2} \right|^2 [I_0(\theta^*) + J_0(\theta^*)], \quad (3.3)$$

where the superscripts c , b , and x refer to coherent, breakup, and charge exchange and the various quantities are as follows.

- | | |
|-----------------|--|
| a_c | Coulomb amplitude |
| a_I, b_I | Non-spin-flip and spin-flip nuclear amplitudes for isospin I in K^+ - N c.m. |
| S_S, S_Q, S_M | Form factors of deuteron (spherical, quadropole, and magnetic) for coherent scattering.
If there were no deuteron d wave, we would have $S_Q = 0$ and $S_M = S_S$ |
| q | Magnitude of momentum transfer $\vec{q} = \vec{k}_0 - \vec{k}$ |
| I_0, J_0 | "Inelastic form factors" for scattering from a deuteron in the initial state to a plane-wave final state |

K Kinematic factor, including the flux factor and the Jacobian for the transformation from $K^+ - N$ c.m. to the laboratory, which reduces to

$$\frac{k^2}{v_0} \frac{dk}{dE_f} \frac{s_{KN}}{\omega_0 \omega E_0 E},$$

where

- k_0, k initial and final momenta of K^+ in the lab
- E_f total energy of $K^+ - d$ final state in the lab
- v_0 velocity of incident K^+ in the lab
- ω_0, ω initial and final lab energy of K^+
- E_0, E initial and final lab energy of "stuck nucleon"
- s_{KN} square of total energy in $K^+ - N$ c.m.

The coherent form factors computed from the Reid wave functions are shown in Fig. 7 together with those obtained from the Hulthén²⁴ wave function (s wave only) and the s -wave part of the Moravscik-Gartenhaus²⁵ wave function. The inelastic form factors I_0 and J_0 were computed from the s -wave part of the Moravscik-Gartenhaus function²⁶ (Fig. 8).

In the derivation of the expressions for the differential cross sections given above, one encounters integrals of K^+ -nucleon matrix elements over the Fermi-momentum distribution of the nucleons within the deuteron. The form-factor approximation rests on the observation that the scattering amplitudes and kinematic factors vary only slightly over the range of these integrals, and can thus be removed from the integrands and evaluated at a typical nucleon momentum; the remaining integrals are then the form factors. Past analyses have used zero for the typical nucleon momentum.¹⁰ In analyzing the coherent scattering, we attempted to evaluate the matrix elements and kinematic factors at a point which is closer to the peak of the integrand (overlap of two deuteron wave functions with different momenta). In particular, we required that momentum be conserved throughout, and that the momentum of the spectator nucleon not change. Thus, both nucleons of the deuteron are in motion prior to the scattering, with initial momentum linked to the scattering angle of the K . The above condition does not uniquely determine the initial nucleon motion; taking the direction of this motion to lie along the momentum-transfer vector maximizes the overlap integral. Figure 9 shows the effects of this description.

C. Energy-independent phase-shift analysis

The data were analyzed using a partial-wave expansion.²⁷ The isospin amplitudes of Eqs. (3.1),

TABLE III. Laboratory breakup differential-cross-section data. These differential cross sections do not include the overall normalization error, which is $\pm 5\%$ at 342 and 479 MeV/c, and $\pm 10\%$ at 587 MeV/c.

$\cos\theta$ interval	No. of events	Correction factor	$d\sigma/d\Omega$ (mb/srad)
587 MeV/c			
(-1.0, -0.7)	28	1.0	0.17 ± 0.03
(-0.7, -0.4)	37	1.0	0.47 ± 0.08
(-0.4, -0.2)	37	1.0	0.71 ± 0.11
(-0.2, 0.0)	36	1.0	0.69 ± 0.11
(0.0, 0.2)	48	1.0	0.92 ± 0.13
(0.2, 0.4)	82	1.0	1.57 ± 0.17
(0.4, 0.6)	106	1.0	2.03 ± 0.20
(0.6, 0.8)	148	1.0	2.84 ± 0.23
(0.8, 0.9)	83	1.0	3.18 ± 0.35
(0.9, 0.95)	34	1.3 ± 0.06	1.69 ± 0.29
470 MeV/c			
(-1.0, -0.7)	51	1.0	0.22 ± 0.03
(-0.7, -0.4)	115	1.0	0.50 ± 0.05
(-0.4, -0.2)	110	1.0	0.72 ± 0.07
(-0.2, 0.0)	119	1.0	0.78 ± 0.07
(0.0, 0.2)	147	1.0	0.97 ± 0.08
(0.2, 0.4)	195	1.0	1.28 ± 0.09
(0.4, 0.6)	244	1.0	1.60 ± 0.10
(0.6, 0.8)	336	1.0	2.21 ± 0.12
(0.8, 0.9)	142	1.0	1.87 ± 0.16
(0.9, 0.95)	54	1.29 ± 0.06	1.83 ± 0.25
342 MeV/c			
(-1.0, -0.7)	48	1.0	0.23 ± 0.03
(-0.7, -0.4)	87	1.0	0.42 ± 0.05
(-0.4, -0.2)	97	1.0	0.71 ± 0.07
(-0.2, 0.0)	106	1.0	0.77 ± 0.08
(0.0, 0.2)	114	1.0	0.83 ± 0.08
(0.2, 0.4)	182	1.0	1.33 ± 0.10
(0.4, 0.6)	196	1.0	1.43 ± 0.10
(0.6, 0.8)	222	1.0	1.62 ± 0.11
(0.8, 0.9)	87	1.0	1.26 ± 0.14

TABLE IV. Charge-exchange differential-cross-section data in the K^*N center of mass (assuming a stationary target nucleon).

$\cos\theta$ interval	No. of events	Correction factor	$d\sigma/d\Omega$ (mb/srad)	σ_{total} (mb)
587 MeV/c				
(-1.0, -0.8)	10	1.52 ± 0.18	0.24 ± 0.07	
(-0.8, -0.6)	12	1.62 ± 0.24	0.35 ± 0.09	
(-0.6, -0.4)	10	1.47 ± 0.17	0.61 ± 0.13	
(-0.4, -0.2)	25	1.37 ± 0.15	0.46 ± 0.10	
(-0.2, 0.0)	35	1.32 ± 0.15	0.59 ± 0.12	
(0.0, 0.2)	42	1.26 ± 0.14	0.69 ± 0.13	
(0.2, 0.4)	36	1.24 ± 0.14	0.59 ± 0.12	
(0.4, 0.6)	45	1.22 ± 0.13	0.71 ± 0.13	
(0.6, 0.8)	31	1.21 ± 0.13	0.48 ± 0.10	
(0.8, 1.0)	23	1.20 ± 0.13	0.34 ± 0.08	6.36 ± 0.56
470 MeV/c				
(-1.0, -0.8)	5	1.60 ± 0.19	0.09 ± 0.04	
(-0.8, -0.6)	14	1.42 ± 0.17	0.23 ± 0.07	
(-0.6, -0.4)	20	1.29 ± 0.14	0.30 ± 0.08	
(-0.4, -0.2)	22	1.37 ± 0.15	0.35 ± 0.08	
(-0.2, 0.0)	36	1.21 ± 0.13	0.51 ± 0.10	
(0.0, 0.2)	32	1.21 ± 0.13	0.45 ± 0.09	
(0.2, 0.4)	30	1.17 ± 0.13	0.41 ± 0.09	
(0.4, 0.6)	29	1.15 ± 0.13	0.39 ± 0.08	
(0.6, 0.8)	36	1.14 ± 0.13	0.48 ± 0.10	
(0.8, 1.0)	12	1.15 ± 0.13	0.16 ± 0.05	4.27 ± 0.36
342 MeV/c				
(-0.1, -0.8)	8	1.62 ± 0.19	0.10 ± 0.04	
(-0.8, -0.6)	9	1.53 ± 0.18	0.10 ± 0.04	
(-0.6, -0.4)	14	2.71 ± 0.19	0.28 ± 0.14	
(-0.4, -0.2)	25	1.46 ± 0.17	0.27 ± 0.06	
(-0.2, 0.0)	31	1.37 ± 0.16	0.32 ± 0.07	
(0.0, 0.2)	30	1.30 ± 0.14	0.29 ± 0.06	
(0.2, 0.4)	25	1.24 ± 0.14	0.23 ± 0.05	
(0.4, 0.6)	36	1.21 ± 0.13	0.32 ± 0.06	
(0.6, 0.8)	33	1.18 ± 0.13	0.29 ± 0.06	
(0.8, 1.0)	13	1.16 ± 0.13	0.11 ± 0.03	2.93 ± 0.24
252 MeV/c				
(-1.0, -0.8)	3	0.42 ± 0.09	0.05 ± 0.03	
(-0.8, -0.6)	5	0.48 ± 0.08	0.08 ± 0.04	
(-0.6, -0.4)	11	0.55 ± 0.07	0.19 ± 0.06	
(-0.4, -0.2)	15	0.64 ± 0.08	0.17 ± 0.05	
(-0.2, 0.0)	22	0.63 ± 0.08	0.26 ± 0.06	
(0.0, 0.2)	19	0.71 ± 0.08	0.20 ± 0.05	
(0.2, 0.4)	18	0.75 ± 0.08	0.17 ± 0.04	
(0.4, 0.6)	19	0.67 ± 0.12	0.21 ± 0.06	
(0.6, 0.8)	24	0.79 ± 0.09	0.22 ± 0.05	
(0.8, 1.0)	5	0.80 ± 0.09	0.05 ± 0.02	1.99 ± 0.18

(3.2), and (3.3) can be expanded in a series of partial waves:

$$a_I(\cos\theta) = \sum_{l=0}^{\infty} \left[(l+1)\alpha_{l+}^I + l\alpha_{l-}^I \right] P_l^I(\cos\theta),$$

$$b_I(\cos\theta) = \sum_{l=0}^{\infty} \left[\alpha_{l+}^I - \alpha_{l-}^I \right] P_l^I(\cos\theta),$$

$$\alpha_{l\pm}^I = \frac{1}{k_{\text{c.m.}}} e^{i\delta_{l\pm}^I} \sin\delta_{l\pm}^I,$$

where the $+$, $-$ subscripts on the partial-wave amplitudes α and phase shifts δ refer to $J = l \pm \frac{1}{2}$, and $k_{\text{c.m.}}$ is the wave number corresponding to the $K^+ - N$ c.m. momentum. At these energies, the

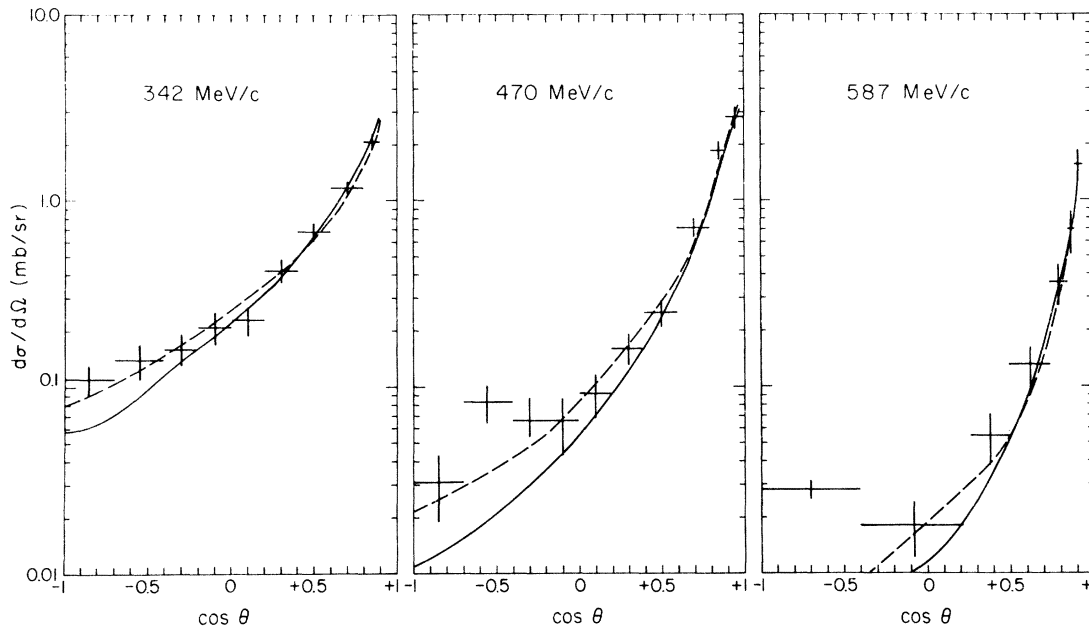


FIG. 3. Observed K^+d coherent differential cross sections in the laboratory frame. The solid line is the combined fit to both coherent and charge-exchange data. The dashed line is a fit to this data only. Not all data which appear in the plots have been included in the fits. (See Tables VI and VII.)

phase shifts can be regarded as real. In this analysis the $I=1$ scattering was considered to be purely s -wave at all momenta studied.²⁸ The values of the $I=1$ phase shifts are listed in Table V. In our analysis these phase shifts were not varied, since their errors are very small compared to the final $I=0$ phase-shift errors.

D. Results of the phase-shift analysis

The phase-shift analysis has been carried out for charge-exchange and coherent scattering. Fits

to the data were attempted for each reaction separately, and for the two combined. The results of the analysis are presented in Tables VI and VII. Reid hard-core form factors were used for the coherent scattering with both stationary- and moving-nucleon kinematics. The Gartenhaus form factor (very similar to the Reid hard-core) with stationary nucleon was used for the charge-exchange cross-section analyses.²⁶ In addition, Table VII contains the results of a fit at 470 MeV/c, using Hulthén wave functions throughout to illustrate the sensitivity of the phase-shift so-

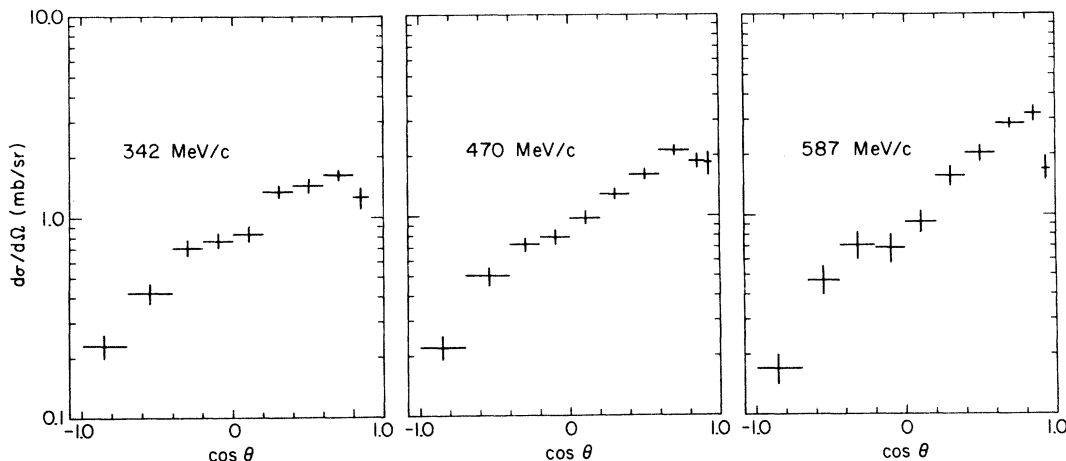


FIG. 4. Plot of observed breakup differential cross sections in the laboratory frame.

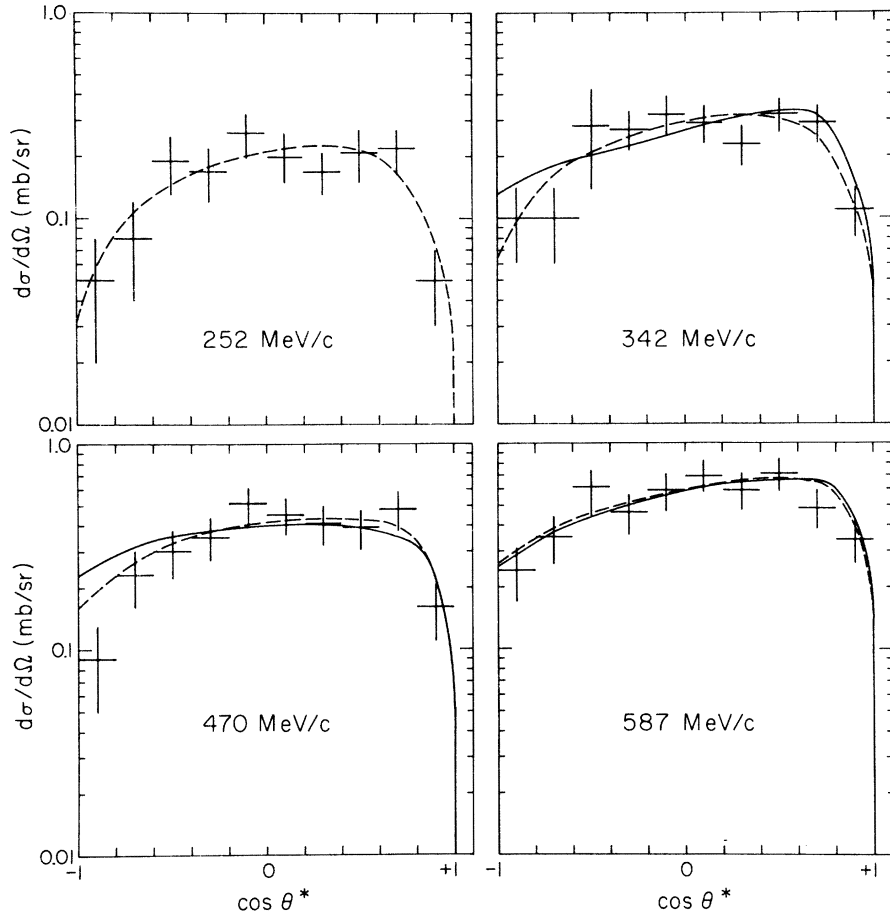


FIG. 5. Observed K^+d charge-exchange differential cross sections in the K^+ -nucleon center-of-mass frame. The solid line is the combined fit to both coherent and charge-exchange data. The dashed line is a fit to this data only.

lutions to the assumed deuteron wave function. It is impossible to distinguish between the different descriptions on the basis of this data alone. No reasonable model can reproduce the structure observed in the tail of the 470-MeV/c coherent distribution shown in Fig. 3. Only coherent scattering with $|t| < 0.4$ (GeV/c) 2 has been included in the fits. (This affects only the 470 and 587 MeV/c data.) In the charge-exchange analysis, the Hulthén and Gartenhaus form factors, assuming a stationary struck nucleon, give similar results. Most fits were performed with only s and p waves, since preliminary trials had shown no convincing need for d waves in the $I=0$ amplitudes. At each momentum two solutions were found, corresponding to the Fermi-Yang ambiguity, i.e., $(\delta_{03} - \delta_{01})_{\text{Fermi}} = -(\delta_{03} - \delta_{01})_{\text{Yang}}$.

It will be seen that the phase shifts obtained from the coherent analysis alone are generally much larger than those from either the charge-exchange or the combined fits. One can see from Eq. (3.1)

and Figs. 7 and 9 that the shape of the coherent angular distribution is dominated by the deuteron form factor and the $I=1$ component in the coherent scattering; thus a sizeable change in the $I=0$ phase shifts is required to significantly affect the differential cross section, and large phase shifts can therefore be obtained. The phase shifts from the combined fits are more tightly constrained and are in better agreement with other experiments.^{10,22} Figures 3–5 display plots of the data and fits to the coherent and charge-exchange differential scattering cross section for each reaction separately and for the combined fit. The phase-shift solutions were obtained from a minimization procedure which has been described elsewhere.¹³

E. Comparison of the phase-shift analysis with other experiments

The $I=0$ phase-shift solutions from other analyses are presented in Table VIII along with our

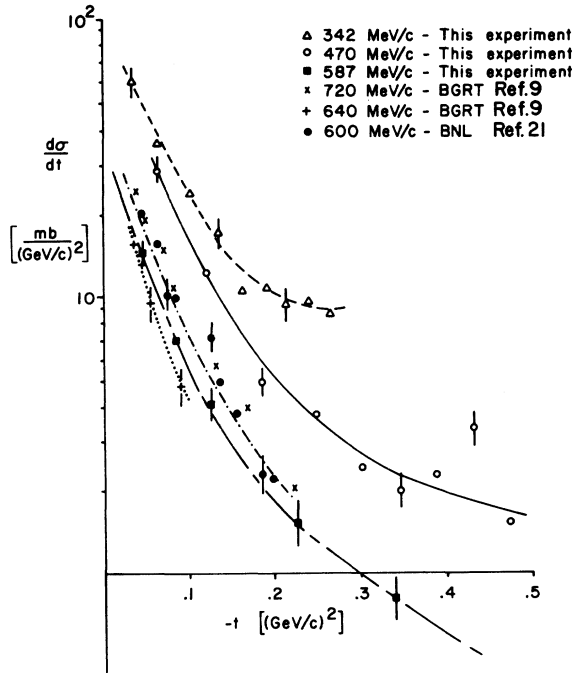


FIG. 6. A plot of the elastic $d\sigma/dt$ as measured in this experiment. Data from other experiments at slightly higher momenta are also shown.

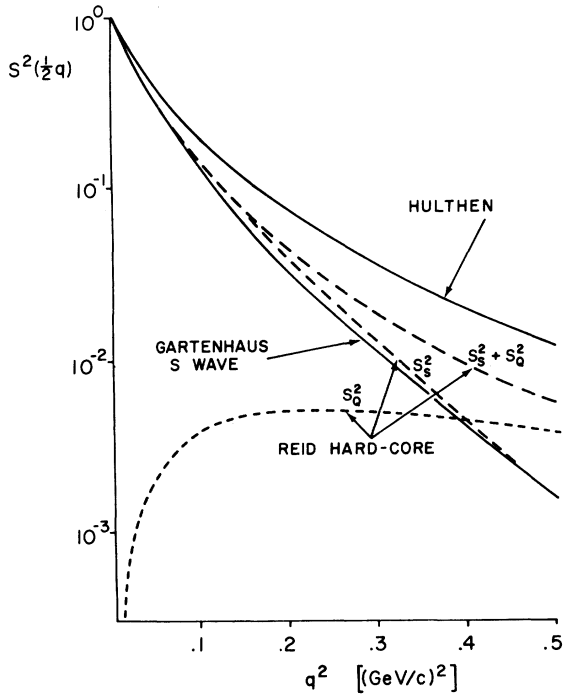


FIG. 7. Deuteron coherent form factors computed from different wave functions as indicated. The factor $(S_s^2 + S_Q^2)$ enters into the non-spin-flip contribution to the differential cross section. For the models with no deuteron d wave $S_Q = 0$. Definitions of form factors are in Ref. 30.

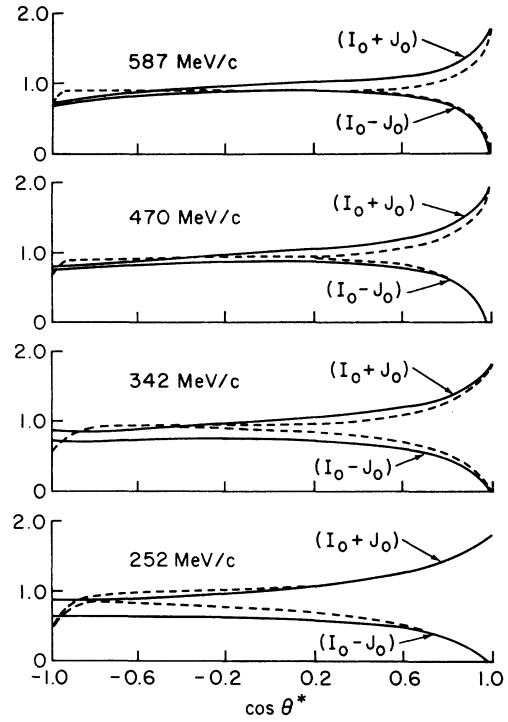


FIG. 8. Form factors $I^0(\theta^*)$ and $J_0(\theta^*)$ vs $\cos\theta^*$ calculated using the Hulthén wave function. The dashed curves at each momentum are the same form factors calculated using the Moravcsik-Gartenhaus wave function.

solutions. The BGRT¹¹ class A, C, and D solutions are from an energy-dependent analysis which did not actually include any experimental data below 600 MeV/c; however, the results are compatible with those they obtained from an energy-independent analysis including the data of Stenger¹⁰ and Lee.²⁸ The values shown in the table were interpolated from the published amplitudes. The analysis by Stenger¹⁰ included both his own data (the sum of the coherent and breakup reactions) and that of Lee²⁹ (charge-exchange); the scattering data at 330 MeV/c and 388 MeV/c were combined at a nominal 350 MeV/c. Even with d waves, Stenger did not have solutions at this momentum with confidence level greater than 1%, the χ^2 being

TABLE V. Isospin $I=1$ s -wave phase shifts.

K^+ lab momentum (MeV/c)	δ_1
252	$-15.0^\circ \pm 0.4^\circ$
342	$-19.5^\circ \pm 0.4^\circ$
470	$-26.8^\circ \pm 0.6^\circ$
587	$-33.4^\circ \pm 0.8^\circ$

TABLE VI. Phase-shift solutions for individual reactions.

Momentum (GeV/c)	δ_0 (deg)	δ_{01} (deg) (Fermi-Yang)	δ_{03} (deg) (Fermi-Yang)	Confidence level	$(\cos\theta)_{\min}$
(a) Coherent scattering					
(1) Reid hard-core form factors, moving nucleon					
342	-3 ± 5	-9 ± 4 51 ± 10	34 ± 6 8 ± 4	0.73	-1.0
470	-19 ± 7	6 ± 16 51 ± 12	39 ± 9 18 ± 12	0.63	-0.4
587	7 ± 11	13 ± 15 31 ± 14	30 ± 6 22 ± 14	0.88	-0.4
(2) Reid hard-core form factors, stationary nucleon					
341	6 ± 5	-17 ± 3 52 ± 9	31 ± 6 4 ± 4	0.70	-1.0
470	-8 ± 7	-8 ± 13 61 ± 13	40 ± 11 12 ± 11	0.65	-0.4
587	19 ± 19	22 ± 33 32 ± 12	24 ± 14 17 ± 12	0.88	
(b) Charge-exchange scattering (Gartenhaus form factors)					
252	5 ± 9	10 ± 8 -5 ± 3	-1 ± 1 7 ± 4	0.63	
342	-6 ± 11	16 ± 10 -8 ± 3	-2 ± 1 10 ± 6	0.70	
470	-2 ± 5	23 ± 5 -12 ± 3	-3 ± 2 14 ± 3	0.27	
587	13 ± 8	27 ± 9 -14 ± 5	-3 ± 2 16 ± 5	0.51	

TABLE VII. Phase-shift results for combined fit to coherent and charge-exchange scattering.

Momentum (GeV/c)	δ_0 (deg)	δ_{01} (deg) (Fermi-Yang)	δ_{03} (deg) (Fermi-Yang)	Confidence level	$(\cos\theta)_{\min}$
(a) With Reid hard-core, moving nucleon for coherent, Gartenhaus for charge exchange					
342	-10 ± 2	-6 ± 1 20 ± 1	14 ± 1 1 ± 1	0.10	-1.0
470	-14 ± 4	-15 ± 2 32 ± 3	19 ± 2 -2 ± 2	0.08	-0.4
587	16 ± 7	-12 ± 5 24 ± 8	15 ± 5 -3 ± 2	0.73	0.25
(b) With Reid hard-core, stationary nucleon for coherent, Gartenhaus for charge exchange					
342	-6 ± 2	-7 ± 1 18 ± 2	12 ± 1 0 ± 1	0.47	-1.0
470	-10 ± 3	-14 ± 2 30 ± 3	18 ± 2 -3 ± 2	0.33	-0.4
587	17 ± 7	-11 ± 5 23 ± 8	14 ± 5 -2 ± 2	0.72	0.25
(c) With Hulthen, stationary nucleon for coherent, Hulthen for charge exchange					
342	2 ± 2	-4 ± 3 9 ± 3	6 ± 2 -1 ± 1	0.8	-1.0
470	2 ± 3	-13 ± 2 $+20 \pm 4$	11 ± 2 -4 ± 1	0.54	-0.4
587	7 ± 6	-17 ± 3 34 ± 6	20 ± 4 -3 ± 2	0.63	0.25

TABLE VIII. $I=0$ phase-shift solutions from previous experiments.

Analysis	Solution No.	s	p_1	p_3	d_3	d_5
342 MeV/c						
BGRT ^a	A	7°	-3.8°	3.8°	0°	0°
	C	2°	9.2°	-1.6°	0.8°	0°
	D	2.9°	10.3°	-1.6°	0.2°	0°
Stenger <i>et al.</i> ^b	<i>sp1</i>	3.8° ± 1.2°	2.5° ± 14.9°	3.1° ± 7.6°		
	<i>sp2</i>	3.8° ± 1.2°	3.2° ± 15.2°	2.7° ± 7.5°		
	<i>spd1</i>	2.3° ± 2.1°	-1.3° ± 2.0°	7.2° ± 2.3°	0.8° ± 1.1°	-3° ± 1°
	<i>spd2</i>	2.3° ± 2.1°	9.8° ± 3.5°	1.5° ± 1.2°	-3.7° ± 1.6°	0.1° ± 0.8°
This expt. combined ^c	1	-9.7° ± 1.8°	-5.9° ± 1.3°	13.6° ± 1.0°		
	2	-9.7° ± 1.8°	20.3° ± 1.3°	0.8° ± 0.9°		
470 MeV/c						
BGRT	A	15.1°	-6.3°	7.2°	-1°	-1°
	C	-3.2°	18.4°	-3.1°	2°	0°
	D	-7.7°	19.1°	3.1°	2°	0°
Stenger <i>et al.</i> ^b	<i>sp1</i>	5.5° ± 2.7°	-10.6° ± 9.1°	9.2° ± 5.2°		
	<i>sp2</i>	5.5° ± 2.7°	16.4° ± -9.7°	-3.4° ± 6.2°		
	<i>spd1</i>	5.9° ± 3.2°	-5.6° ± 3.9°	13.0° ± 3.0°	-1.5° ± 2.3°	-7.1° ± ?
	<i>spd2</i>	5.9° ± 3.2°	19.3° ± 5.0°	0.8° ± 2.3°	-8.2° ± 3.0°	-2.7° ± ?
This expt. combined ^c	1	-13.6° ± 3.5°	-14.5° ± 2.3°	19.4° ± 1.8°		
	2	-13.6° ± 3.5°	32.0° ± 2.6°	-1.9° ± 1.6°		
587 MeV/c						
BGRT ^a	A	22.6°	-7.9°	9.5°	-1.6°	-3.2°
	C	-5.6°	25.6°	-3.9°	4.3°	-5.0°
	D	-10.6°	25.7°	-4.4°	4.3°	0°
Ray <i>et al.</i> ^d		6.0° ± 7.6°	30.3° ± 6.4°	-2.7° ± 3.2°		
Stenger <i>et al.</i> ^b	<i>sp1</i>	10.7° ± 11.5°	-18.0° ± 5.3°	14.5° ± 12.6°		
	<i>sp2</i>	10.7° ± 11.5°	27.4° ± 12.7°	-5.7° ± 3.8°		
	<i>spd1</i>	6.6° ± 4.9°	7.5° ± 12.3°	21.0° ± 3.9°	1.8° ± 5.3°	7.5° ± 6
	<i>spd2</i>	6.7° ± 4.9°	3.2° ± 8.0°	1.4° ± 6.2°	7.8° ± 9.2°	-3.0° ± ?
This expt. combined ^c	1	15.5° ± 7.0°	-12.2° ± 4.5°	14.8° ± 4.8°		
	2	15.5° ± 7.0°	24.4° ± 8.2°	-2.6° ± 1.8°		

^aInterpolated from amplitudes listed in Ref. 11.

^bValues for 342 MeV/c are Stenger's (Ref. 10) 350-MeV/c results; those for 470 MeV/c are scaled down from his 530-MeV/c phase shifts. Stenger had no solutions at 350 MeV/c with confidence level >1%.

^cNo d waves were included since the data could be fitted extremely well without them.

^dSee Ref. 22.

dominated by the low forward bin. His solutions for 520 MeV/c were scaled down to yield the ones shown in the table. Finally, our solutions are presented from the energy-independent fits to our combined data. (See Fig. 10.)

It will be noticed that the phase shifts are mostly small, with the exceptions of the p_{01} phase shifts in the Yang-type solutions, and the s -wave part of the BGRT A solution; and even these are far smaller than the p -wave phase shifts found in the coherent scattering analysis of Table VI.

A comparison of our solutions 1 and 2 at 587

MeV/c with the phase-shift analysis, based on polarization information of Ray *et al.*,²² indicates that the Fermi-Yang ambiguity (solutions 1 and 2) is resolved in favor of solution 2. Our best description of $I=0$ $K+N$ scattering below 600 MeV/c is therefore given by our solution 2 in Table VIII.³⁰

IV. SUMMARY AND CONCLUSION

In the analysis of the K^+ reactions we use the results of our recent K^+p scattering experiment¹³ which indicate that, for the $I=1$ amplitude, only

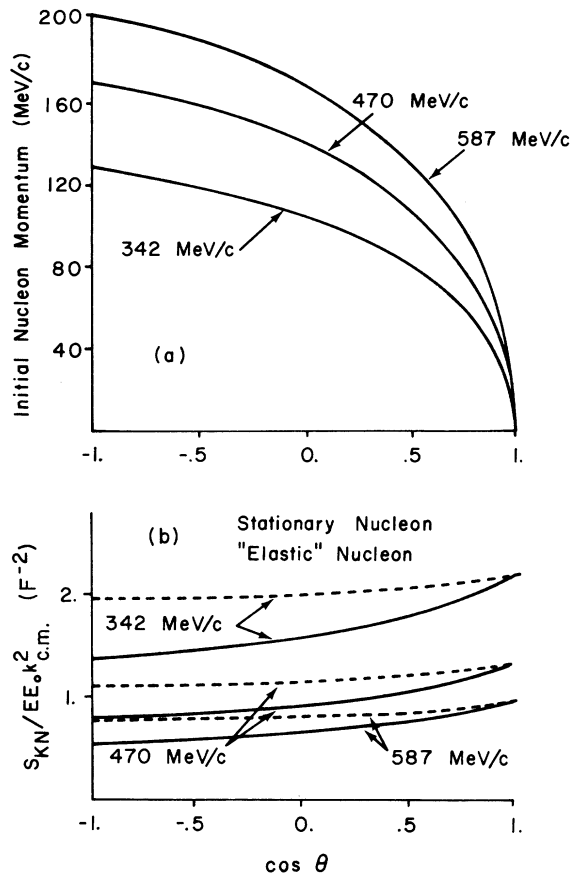


FIG. 9. Kinematic effects of the moving-nucleon description of coherent scattering (see text), as a function of the K^+ lab scattering angle. (a) Initial lab momentum of the struck nucleon in this model; direction is opposite that of the momentum-transfer vector. (b) The kinematic factors in the elastic differential-cross-section expression which depend on the description used for the nucleon motion.

the lowest partial wave is required to fit the data. With this starting point, a consistent description of K^+d charge-exchange and coherent scattering at three momenta below 600 MeV/c, and of the charge-exchange scattering at 252 MeV/c, is obtained by including only s and p waves in the $I=0$ amplitude. Using the single-scattering impulse approximation, two solutions, the Fermi-Yang set, were found in each momentum interval.

These results are in disagreement with Ray *et al.*,²² who require s , p , and d waves in the $I=0$ amplitude or s and p waves in both $I=0$ and $I=1$ amplitudes to fit his data which, however, include polarization data favoring the Yang solution. These results are also in disagreement with Stenger,¹⁰ who fit the charge-exchange data of Lee²⁹ in conjunction with his own data on coherent and breakup reactions and found that d waves were necessary

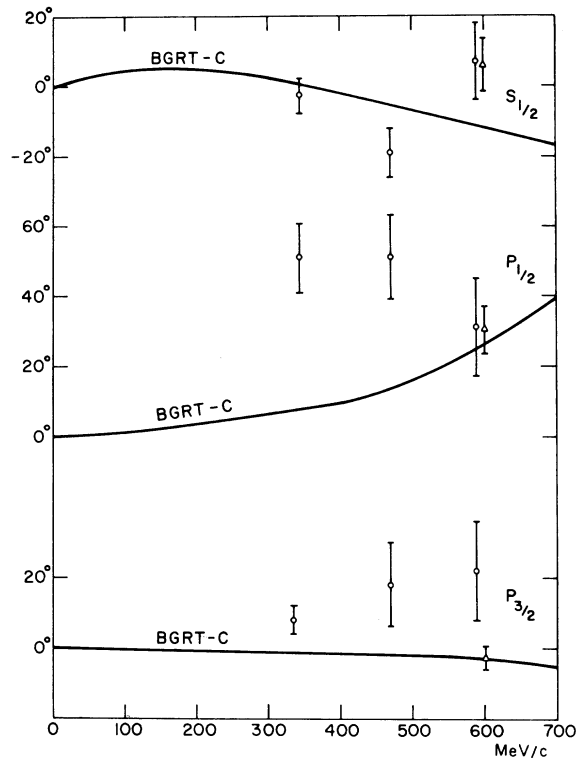


FIG. 10. Momentum dependence of combined phase-shift solutions from this experiment (circles). The BGRT phase-shift solutions and the data of Ref. 22 (triangles) are included for comparison.

at 530 and 330 MeV/c. On the other hand, Stenger's s - and p -wave-only solutions at these momenta, while giving poor values of χ^2 for his data, agree for the most part with our solutions.

The data of this experiment could be adequately fitted with a model in which the form factors were all calculated using Hulthén wave functions. In our final analysis, we used a more realistic set of form factors, based on the Moravcsik-Gartenhaus and Reid hard-core deuteron wave functions.²⁶ In order to obtain satisfactory fits to the data it was necessary to eliminate the large-angle scattering [$|t| > 0.4$ (GeV/c)²] at the higher momenta.

It is possible that the leveling off of the differential cross sections beyond 90° is evidence that double scattering is becoming important relative to single scattering.³¹ This would indicate that the use of, say, the Hulthén form factor, with its large contribution in the backward region, compensates for the omission of double-scattering terms in the model and thus "accidentally" produces phase shifts in agreement with the data. With the limited coherent-scattering data of this experiment, however, the evidence for the necessity of double-scattering terms is by no means

established.

In this experiment the coherent and breakup reactions have been separated for the first time in this energy region, and the differential cross sections for these processes determined. While the total non-charge-exchange cross section is approximately constant over the momentum range included in this analysis, the ratio of coherent to breakup cross sections is rapidly decreasing.

ACKNOWLEDGMENTS

We would like to thank Dr. V. R. Veirs, Dr. T. B. Day, Dr. B. Kehoe, J. Wallace, and J. LeFebvre for their valuable assistance in early phases of this work. We also wish to acknowledge the efforts of the many members of the bubble-chamber groups at Maryland and IIT, especially C. Aaron, E. Dann, M. Kocik, and G. Parks.

*Work supported in part by the U. S. Energy Research and Development Administration and the National Science Foundation.

†Present address: Moshman Associates, Inc., Bethesda, Maryland.

‡Present address: Computer Sciences, Corporation, Silver Spring, Maryland.

- ¹R. L. Cool, G. Giacomelli, T. F. Kycia, B. A. Leontic, K. K. Li, A. Lundby, and J. Teiger, *Phys. Rev. Lett.* **17**, 102 (1966).
- ²D. V. Bugg, R. S. Gilmore, K. M. Knight, D. C. Salter, G. H. Stafford, E. J. Wilson, J. D. Davies, J. D. Dowell, P. M. Hattersley, R. J. Homer, A. W. O'Dell, A. A. Carter, R. J. Tapper, and K. F. Riley, *Phys. Rev.* **168**, 1466 (1968).
- ³R. J. Abrams, R. L. Cool, G. Giacomelli, T. F. Kycia, B. A. Leontic, K. K. Ki, and D. N. Michael, *Phys. Rev. D* **1**, 1917 (1970).
- ⁴T. Bowen, P. K. Caldwell, F. Ned Dikmen, E. W. Jenkins, R. M. Kalbach, D. V. Petersen, and A. E. Pifer, *Phys. Rev. D* **2**, 2599 (1970).
- ⁵R. L. Cool, G. Giacomelli, T. F. Kycia, B. A. Leontic, K. K. Li, A. Lundby, and C. Wilkin, *Phys. Rev. D* **1**, 1887 (1970).
- ⁶T. Bowen, E. W. Jenkins, R. M. Kalbach, D. V. Petersen, A. E. Pifer, and P. K. Caldwell, *Phys. Rev. D* **7**, 22 (1973).
- ⁷J. D. Dowell, in *Proceedings of the XVI International Conference on High Energy Physics, Chicago-Batavia, Ill., 1972*, edited by J. D. Jackson and A. Roberts (NAL, Batavia, Ill., 1973), and references therein.
- ⁸A. T. Lea, B. R. Martin, and G. C. Oades, *Phys. Rev.* **165**, 1968 (1970).
- ⁹W. Cameron, A. A. Hirata, R. Jennings, W. T. Morton, E. Cazolli, G. Giacomelli, P. Lugaresi-Serra, G. Mandrioli, A. Minguzzi-Ranzi, E. Castelli, M. Furlan, P. Poropat, C. Omera, and M. Sessa, *Nucl. Phys.* **B78**, 93 (1974).
- ¹⁰V. J. Stenger, W. E. Slater, D. H. Stork, H. K. Ticho, G. Goldhaber, and S. Goldhaber, *Phys. Rev.* **134B**, 1111 (1964); and V. J. Stenger, Ph.D. thesis, UCLA, 1963 (unpublished).
- ¹¹G. Giacomelli, P. Lugaresi-Serra, G. Mandrioli, A. M. Rossi, F. Griffiths, I. M. Hughs, D. A. Jacobs, R. Jennings, B. C. Wilson, G. Ciapetti, V. Costantini, G. Martellotti, D. Zanello, E. Costellani, and M. Sessa, *Nucl. Phys.* **B20**, 301 (1970); G. Giacomelli, P. Lugaresi-Serra, G. Madrioli, A. Minguzzi-Ranzi, A. M. Rossi, F. Griffiths, A. A. Hirata, I. S. Hughes, R. Jennings, B. C. Wilson, G. Ciapetti, G. Mastantonio, A. Nappi, D. Zanello, G. Alberi, E. Costelli, P. Poropat, and M. Sesson, *Nucl. Phys.* **B71**, 138 (1974) and references therein (referred to as the BGRT group).
- ¹²R. Aaron, M. Rich, W. L. Hogan and Y. N. Srivastava, *Phys. Rev. D* **7**, 1401 (1973).
- ¹³R. A. Burnstein, J. J. LeFebvre, D. V. Petersen, H. A. Rubin, T. B. Day, J. R. Fram, R. G. Glasser, G. E. McClellan, B. Sechi-Zorn, and G. A. Snow, *Phys. Rev.* **10**, 2767 (1974).
- ¹⁴D. Berley, Brookhaven National Laboratory AGS Internal Report No. DB-1, 1963 (unpublished).
- ¹⁵T. B. Day, University of Maryland Technical Report No. 649, 1966 (unpublished).
- ¹⁶B. Kehoe and D. G. Hill, University of Maryland Technical Report No. 75-005, 1974 (unpublished).
- ¹⁷G. R. Rosenblatt, Ph.D. thesis, Illinois Institute of Technology, Technical Report No. 127, 1974 (unpublished).
- ¹⁸D. E. Trevett, Ph.D. thesis, University of Maryland Technical Report No. 75-037, 1974 (unpublished).
- ¹⁹Particle Data Group, *Rev. Mod. Phys.* **45**, 51 (1973).
- ²⁰G. Giacomelli, P. Lugaresi-Serra, G. Mandrioli, A. Minguzzi-Ranzi, F. Griffiths, A. A. Hirata, I. S. Hughes, R. Jennings, B. C. Wilson, G. Ciapetti, G. Mastantonio, D. Zanello, G. Alberi, E. Castelli, P. Poropat, and M. Sessa, *Nucl. Phys.* **B68**, 285 (1974).
- ²¹M. Sakitt, J. Shelley, and J. A. Thompson, Brookhaven National Laboratory Report No. 19029, 1974 (unpublished).
- ²²A. K. Ray, R. W. Burris, H. E. Fisk, R. W. Kraemer, D. G. Hill, and M. Sakitt, *Phys. Rev.* **183**, 1185 (1969).
- ²³R. V. Reid, Jr., *Ann. Phys. (N.Y.)* **50**, 411 (1968).
- ²⁴L. Hulthén and M. Sugawara, in *Structure of Atomic Nuclei, Vol. XXXIX of Handbuch der Physik*, edited by S. Flügge (Springer, Berlin, 1957), p. 1.
- ²⁵G. Giacomelli (private communication) has provided the results of the form-factor calculations of G. Mandrioli, G. Alberi, and P. Poropat.
- ²⁶J. D. Jackson and J. M. Blatt, *Rev. Mod. Phys.* **22**, 77 (1950); M. L. Goldberger and K. M. Watson, *Collision Theory* (Wiley, New York, 1964).
- ²⁷The description of $I=1$ scattering as due to s waves is based on the results of a recent IIT-Maryland experiment on low-energy K^+p scattering (Ref. 13) which was undertaken to provide improved $I=1$ data for this K^+d experiment.
- ²⁸W. Lee, W. Chinowsky, G. Goldhaber, S. Goldhaber, T. O'Halloran, W. Slater, D. H. Stork, and H. K. Ticho, *Phys. Rev. Lett.* **7**, 378 (1969); W. Lee, Ph.D. thesis, UCRL-9601, 1961 (unpublished).
- ²⁹R. M. Edelstein, H. E. Fisk, P. Joseph, E. L. Muller, J. S. Russ, M. O. Schick, R. C. Thatcher, D. L. Cheshire, R. C. Lamb, F. C. Peterson, and E. W.

Hoffman, Phys. Rev. D 14, 702 (1976), report a measurement at incident momenta 550 to 700 MeV/c of $d\sigma/dt(K^0 p \rightarrow K^+ n)$ equal to 19 ± 2 mb/GeV² at $t = -0.065$ (GeV/c)². The phase shifts from (a) in Table VII at

0.587 GeV/c predict 20.6 mb/GeV².
³¹C. Michael and C. Wilkin, Nucl. Phys. B11, 99 (1969); D. Sidhu and C. Quigg, Phys. Rev. D 7, 755 (1973).